

OPTICAL AND NEAR-INFRARED SPECTROSCOPY OF THE L SUBDWARF SDSS J125637.13-022452.4

ADAM J. BURGASSER¹, SOEREN WITTE², CHRISTIANE HELLING³, ROBYN E. SANDERSON¹, JOHN J. BOCHANSKI¹, AND PETER H. HAUSCHILDT²

Submitted to ApJ 11 October 2008; Accepted 9 March 2009

ABSTRACT

Red optical and near-infrared spectroscopy are presented for SDSS J125637.13–022452.4, one of only four L subdwarfs reported to date. These data confirm the low-temperature, metal-poor nature of this source, as indicated by prominent metal-hydride bands, alkali lines, and collision-induced H₂ absorption. The optical and near-infrared spectra of SDSS J1256–0224 are similar to those of the sdL4 2MASS J16262034+3925190, and we derive a classification of sdL3.5 based on the preliminary scheme of Burgasser, Cruz, & Kirkpatrick. The kinematics of SDSS J1256–0224 are consistent with membership in the Galactic inner halo, with estimated *UVW* space velocities indicating a slightly prograde, eccentric and inclined Galactic orbit ($3.5 \lesssim R \lesssim 11$ kpc; $|Z_{\max}| = 7.5$ kpc). Comparison to synthetic spectra computed with the PHOENIX code, including the recent implementation of kinetic condensate formation (DRIFT-PHOENIX), indicate $T_{\text{eff}} \approx 2100\text{--}2500$ K and $[M/H] \approx -1.5$ to -1.0 for $\log g \approx 5.0\text{--}5.5$ (cgs), although there are clear discrepancies between model and observed spectra particularly in the red optical region. The stronger metal-oxide bands present in the DRIFT-PHOENIX model spectra, a result of phase-non-equilibrium abundances of grain species, appears to contradict prior suggestions that grain formation is inhibited in metal-poor atmospheres; conclusive statements on the metallicity dependence of grain formation efficiency are as yet premature. In addition, an apparent shift in the temperature scale of L subdwarfs relative to L dwarfs may obviate the need for modified grain chemistry to explain some of the former’s unique spectral characteristics.

Subject headings: stars: chemically peculiar — stars: individual (SDSS J125637.13–022452.4) — stars: low mass, brown dwarfs — subdwarfs

1. INTRODUCTION

L subdwarfs are the lowest-luminosity and least-massive halo population dwarf stars currently known (Burgasser, Kirkpatrick, & Lépine 2005). They derive their name from their gross spectral similarities to the local L dwarf population of very low mass stars and brown dwarfs (see Kirkpatrick 2005), but are distinguished by specific spectral anomalies, including the presence of enhanced metal hydride absorption bands and unusually blue near-infrared colors. These features are indicative of subsolar atmospheric abundances, as similar peculiarities distinguish metal-poor M subdwarfs from M dwarfs (e.g., Mould & Hyland 1976; Gizis 1997; Leggett et al. 2000). L subdwarfs, like M subdwarfs, exhibit kinematics consistent with membership in the Galactic halo, with inclined and eccentric Galactic orbits indicating dynamical heating over long timescales and/or formation outside the Galactic disk (Dahn et al. 2008; Burgasser et al. 2008; Cushing et al. 2009). The low luminosities ($\log L_{\text{bol}}/L_{\odot} < -3$) and effective temperatures of L subdwarfs ($T_{\text{eff}} < 3000$ K; Leggett et al. 2000; Reiners & Basri 2006; Burgasser et al. 2008), coupled with their non-solar atmospheric abundances, are of particular interest for studies of low temperature atmospheres, testing thermochemistry and condensate formation processes in chemically

peculiar environments (e.g., Ackerman & Marley 2001; Lodders 2002; Helling & Woitke 2006). In addition, as their inferred masses extend down to and below the metallicity-dependent hydrogen burning minimum mass (Burrows et al. 1993; Burgasser et al. 2003a), L subdwarfs can potentially test metallicity dependencies on low-mass star formation and brown dwarf evolution, relevant for instance in tracing the terminus of the main sequence in globular clusters (e.g., Richer et al. 2008).

Despite their utility to atmospheric, star formation and Galactic population studies, only four L subdwarfs have been reported to date: the prototype 2MASS J05325346+8246465 (Burgasser et al. 2003a, hereafter 2MASS 0532+8246), 2MASS J16262034+3925190 (Burgasser 2004, hereafter 2MASS J1626+3925), 2MASS J06164006–6407194 (Cushing et al. 2009, hereafter 2MASS J0616–6407), and SDSS J125637.13–022452.4 (Sivarani et al. 2009, hereafter SDSS J1256–0224). The first three sources were identified serendipitously in the Two Micron All Sky Survey (Skrutskie et al. 2006, hereafter 2MASS), and have been studied extensively at optical and near-infrared wavelengths (e.g. Burgasser et al. 2008; Burgasser, Cruz & Kirkpatrick 2007; Cushing & Vacca 2006; Cushing et al. 2009; Gizis & Harvin 2006; Reiners & Basri 2006; Patten et al. 2006; Scholz et al. 2009; Schilbach, Röser & Scholz 2009). SDSS J1256–0224 was found in the Sloan Digital Sky Survey (York et al. 2000, hereafter SDSS) as part of a directed search for unusual red sources. Both Sivarani et al. (2009) and Scholz et al. (2009) have identified SDSS J1256–0224 as an L subdwarf

¹ Massachusetts Institute of Technology, Kavli Institute for Astrophysics and Space Research, Building 37, Room 664B, 77 Massachusetts Avenue, Cambridge, MA 02139, USA; ajb@mit.edu

² Hamburger Sternwarte, Gojenbergsweg 112, 21029 Hamburg, Germany

³ SUPA, School of Physics and Astronomy, University of St. Andrews, North Haugh, St. Andrews KY16 9SS, UK

based on its optical spectrum (L-type, with unusually strong metal hydride bands), blue near-infrared colors ($J - K_s = 0.10 \pm 0.03$; Schilbach, Röser & Scholz 2009), and halo-like kinematics. As yet, no detailed study of the optical and near-infrared spectral properties of this unusual source have been made.

In this article, we present new observations of SDSS J1256–0224 and conduct a detailed analysis of its spectral and kinematic properties. Spectroscopic observations spanning the red optical and near-infrared are described in § 2. The empirical properties of SDSS J1256–0224 are assessed in § 3, including classification (on the preliminary scheme of Burgasser, Cruz & Kirkpatrick 2007), distance estimation, kinematics and Galactic orbit. In § 4 we examine the atmospheric properties of this source by comparing its colors and spectra to the latest generation of the COND-PHOENIX atmosphere simulations (Hauschildt, Baron & Allard 1997) and to the DRIFT-PHOENIX model atmospheres (Dehn 2007; Helling et al. 2008b; Witte 2008), the latter of which includes a kinetic approach of phase-non-equilibrium dust formation. Results are summarized in § 5.

2. OBSERVATIONS

2.1. Red Optical Spectroscopy

Optical spectra of SDSS J1256–0224 were obtained on 2006 May 7 (UT) using the Low Dispersion Survey Spectrograph (LDSS-3) mounted on the Magellan 6.5m Clay Telescope. LDSS-3 is an imaging spectrograph, upgraded from the original LDSS-2 (Allington-Smith et al. 1994) for improved red sensitivity. Conditions during the observations were clear with excellent seeing ($0''.6$ at i' -band). The VPH-red grism (660 lines/mm) with a $0''.75$ wide (4 pixels) longslit mask was used, with the slit aligned to the parallactic angle. This configuration provides 6050–10500 Å spectra across the entire chip with an average resolution of $\lambda/\Delta\lambda \approx 1800$ and dispersion along the chip of ~ 1.2 Å/pixel. The OG590 longpass filter was used to eliminate second order light shortward of 6000 Å. Two slow-read exposures of 750 s each were obtained at an airmass of 1.12. We also observed the G2 V star G 104-335 ($V = 11.7$) immediately after the SDSS J1256–0224 observation and at a similar airmass (1.14) for telluric absorption correction. The flux standard LTT 7987 (a.k.a. GJ 2147; Hamuy et al. 1994) was observed on the same night using an identical slit and grism combination. All spectral observations were accompanied by HeNeAr arc lamp and flat-field quartz lamp exposures for dispersion and pixel response calibration.

LDSS-3 data were reduced in the IRAF⁴ environment (Tody 1986). Raw images were first corrected for amplifier bias voltage, stitched together, and subtracted by a median-combined set of slow-read bias frames taken during the afternoon. These processed images were then divided by a median-combined, bias-subtracted and normalized set of flat field frames. The LTT 7987 and G 104-335 spectra were optimally extracted first using the

APALL task with background subtraction. The spectrum of SDSS J1256–0224 was then extracted using the G star dispersion trace as a template. Dispersion solutions were determined from arc lamp spectra extracted using the same dispersion trace; solutions were accurate to ~ 0.08 pixels, or ~ 0.1 Å. Flux calibration (instrumental response correction) was determined using the tasks STANDARD and SENSFUNC with observations of LTT 7987, which we have found provide sufficient calibration to $<10\%$ over the 6000–9000 Å spectral band (Burgasser, Cruz & Kirkpatrick 2007). Corrections to telluric O₂ (6855–6955 Å B-band, 7580–7740 Å A-band) and H₂O (7160–7340 Å, 8125–8350 Å, 9270–9680 Å) absorption bands were determined by linearly interpolating over these features in the G dwarf spectrum, dividing by the uncorrected spectrum, and multiplying the result with the spectrum of SDSS J1256–0224. The two spectra of SDSS J1256–0224 were then coadded to improve signal-to-noise, which ranged from ~ 15 at the 6600 Å peak to a maximum of ~ 45 at 8500 Å.

The reduced red optical spectrum of SDSS J1256–0224 is shown in Figure 1, compared to equivalent data for the sdM9.5 SSSPM J1013-1356 (Scholz et al. 2004a) and 2MASS J1626+3925 (Burgasser, Cruz & Kirkpatrick 2007).⁵ Our data for SDSS J1256–0224 have considerably higher signal-to-noise than the original SDSS discovery spectrum (Sivarani et al. 2009) and higher resolution than contemporaneous observations by Scholz et al. (2009). As originally pointed out by Sivarani et al. (2009), the optical spectrum of SDSS J1256–0224 exhibits several characteristics indicative of an L dwarf, including an overall red spectral slope from 6000–8500 Å; strong molecular bands of CrH (8600 Å) and FeH (8700 and 9900 Å); and alkali line absorption from K I (7700 Å doublet), Na I (8182/8193 Å doublet), Rb I (7798 and 7946 Å) and Cs I (8519 and possibly 8941 Å). Equivalent width (EW) measurements for these lines are listed in Table 2. The K I doublet is extremely broadened, producing a V-shape notch in the spectrum that spans 7300–8100 Å, also characteristic of L dwarf spectra. There are a number of peculiar features in the spectrum of SDSS J1256–0224 that are not common to L dwarf spectra, however, including unusually strong bands of CaH (6900 Å) and TiO (7200 and 8400 Å), and numerous metal lines from Ca I (6571 Å), Ca II (8541 Å) and Ti I (7204, 8433 and 9600–9700 Å⁶). The absence of these species in L dwarf spectra is largely attributed to the formation of Ca-Ti and Ca-Al mineral condensates (e.g., Allard et al. 2001; Lodders 2002; Helling, Woitke & Thi 2008), and their presence in L subdwarf spectra has been interpreted as an indication of inhibited condensate formation (Burgasser et al. 2003a; Reiners & Basri 2006). Whether or not this is an accurate interpretation (see § 4.3), unusually strong CaH and metal-line ab-

⁵ These data were obtained with the Gemini Multi-Object Spectrometer (Hook et al. 2004).

⁶ Absorption in the 9600–9700 Å spectrum of 2MASS J1626+3925 was incorrectly associated with TiH by Burgasser (2004). Cushing & Vacca (2006) and Reiners & Basri (2006) have since identified these features as arising from the $^5F_z - ^5F_o$ multiplet of Ti I, and we adopt these identifications here.

⁴ IRAF is distributed by the National Optical Astronomy Observatories, which are operated by the Association of Universities for Research in Astronomy, Inc., under cooperative agreement with the National Science Foundation.

sorption is a characteristic trait of metal-poor M subdwarf spectra (e.g., Mould & Hyland 1976; Gizis 1997) and the presence of these features in the spectrum of SDSS J1256–0224 supports its characterization as a metal-poor, low-temperature dwarf.

Specific comparison of SDSS J1256–0224 to 2MASS J1626+3925 reveals remarkable similarities between these two sources, although the latter exhibits somewhat stronger FeH, CrH, Rb I and Cs I absorption features and somewhat weaker Na I lines. Indeed, the variation in features between the three spectra shown in Figure 1 suggests a sequence of very late-type, metal-poor subdwarfs, with SDSS J1256–0224 having intermediate line and band strengths. The specific spectral classification of SDSS J1256–0224 is discussed in detail in § 3.1. Note that no significant H α emission or absorption is detected in any of these spectra.

2.2. Near-Infrared Spectroscopy

Low resolution near-infrared spectral data for SDSS J1256–0224 were obtained in clear conditions on 2005 March 23 (UT) using the SpeX spectrograph (Rayner et al. 2003) mounted on the 3m NASA Infrared Telescope Facility (IRTF). We used the prism-dispersed mode of SpeX with a 0''.5 slit (aligned to the parallactic angle), providing 0.75–2.5 μ m spectroscopy with resolution $\lambda/\Delta\lambda \approx 120$ and dispersion across the chip of 20–30 \AA pixel⁻¹. SDSS J1256–0224 was observed at an airmass of 1.08. Four exposures of 180 s each were obtained in an ABBA dither pattern along the slit. The A0 V star HD 111744 was observed immediately before SDSS J1256–0224 at a similar airmass (1.07) for telluric absorption and flux calibration. Internal flat field and Ar arc lamps were observed with the target and calibrator source for pixel response and wavelength calibration.

Data were reduced using the SpeXtool package, version 3.1 (Cushing, Vacca, & Rayner 2004) using standard settings. Raw science images were first corrected for linearity, pair-wise subtracted, and divided by the corresponding median-combined flat field image. Spectra were optimally extracted using the default settings for aperture and background source regions, and wavelength calibration was determined from arc lamp and sky emission lines. The multiple spectral observations were then median-combined after scaling individual spectra to match the highest signal-to-noise observation. Telluric and instrumental response corrections for the science data were determined using the method outlined in Vacca et al. (2003), with line shape kernels derived from the arc lines. Adjustments were made to the telluric spectra to compensate for differing H I line strengths and pseudo-velocity shifts. Final calibration was made by multiplying the spectrum of SDSS J1256–0224 by the telluric correction spectrum, typically accurate to within 10% across the 0.8–2.5 μ m window (see Burgasser, Kirkpatrick & Burrows 2006). Instrumental response was determined through the ratio of the observed A0 V spectrum to a scaled, shifted and deconvolved Kurucz⁷ model spectrum of Vega. Signal-to-noise ranged from ~ 80 at the J -band peak ($\sim 1 \mu$ m) to ~ 15 at K -band ($\sim 2.2 \mu$ m).

⁷ See <http://kurucz.harvard.edu/stars.html>.

The reduced near-infrared spectrum of SDSS J1256–0224 is shown in Figure 2, again compared to equivalent SpeX prism data for SSSPM J1013-1356 and 2MASS J1626+3925 (Burgasser 2004). All three spectra show similar overall spectral morphologies, with strong molecular absorption features and relatively blue 1.0–2.5 μ m spectral slopes. Again, 2MASS J1626+3925 appears to be most similar to SDSS J1256–0224 in terms of detailed spectral features. The strong FeH band at 0.99 μ m present in the optical spectrum of SDSS J1256–0224 is clearly discerned in these data, intermediate in strength between SSSPM J1013-1356 and 2MASS J1626+3925 but considerably stronger than any normal L dwarf. Strong FeH absorption is also present in the 1.2–1.3 μ m region. H₂O absorption is quite pronounced at 1.4 μ m, but the 1.8 μ m band is notably weaker. CO absorption at 2.3 μ m, a hallmark of M and L dwarf near-infrared spectra, is absent in the three subdwarf spectra shown here. The weakened 1.8 μ m H₂O and 2.3 μ m CO bands, and the overall blue spectral slope, can be attributed to enhanced H₂ absorption in all three sources, peaking at 2.1 μ m but spanning much of the 1.5–2.5 μ m region shown (Linsky 1969; Saumon et al. 1994; Borysow, Jørgensen, & Zheng 1997). This absorption produces the very blue near-infrared color of SDSS J1256–0224, $J - K_s = 0.10 \pm 0.03$ (Schilbach, Röser & Scholz 2009)⁸, quite distinct from the colors of normal L dwarfs ($J - K_s \approx 1.5$ –2.5, Kirkpatrick et al. 2000). Atomic lines arising from the neutral alkalis Na I and K I are also seen, but the resolution of the SpeX prism data is insufficient to obtain meaningful EW measurements.

3. CHARACTERIZATION OF SDSS J1256–0224

3.1. Spectral Classification

The most basic characterization of a late-type dwarf like SDSS J1256–0224 is its spectral classification. However, while a well-defined red optical classification scheme exist for L dwarfs (Kirkpatrick et al. 1999b, 2000; see also Geballe et al. 2002 for discussion on the near-infrared classification of L dwarfs), there are simply too few L subdwarfs to define a robust scheme. We therefore followed the approach outlined in Burgasser, Cruz & Kirkpatrick (2007), comparing the 7300–9000 \AA spectrum of SDSS J1256–0224 to equivalent-resolution spectra of the L dwarf spectral standards defined in Kirkpatrick et al. (1999b). Figure 3 shows the two best-matching standards, the L3 2MASS J11463449+2230527 and the L4 2MASS J11550087+2307058 (data from Kirkpatrick et al. 1999b⁹). Focusing on the 7300–9000 \AA region, the spectrum of SDSS J1256–0224 appears to lie intermediate between these two standards, based on the height of the 7300 \AA spectral peak; the depth and breadth of the 7700 \AA K I doublet; and the depths of the 8500 \AA TiO, 8600 \AA CrH and 8700 \AA FeH bands. There are discrepancies between SDSS J1256–0224 and the L dwarf standards in this region, notably the spectral

⁸ Note that the 2MASS $J - K_s = 0.66$ color reported by Sivarani et al. (2009) is in fact an upper limit; this source was not detected by 2MASS in the K_s band.

⁹ These data were obtained with the Low Resolution Imaging Spectrograph (Oke et al. 1995).

slope between 7800 Å and 8400 Å, the depth of the 8200 Å Na I doublet (stronger in SDSS J1256–0224), and the presence of additional Ca I, Ca II and Ti I lines in the spectrum of SDSS J1256–0224. However, these differences are not nearly as extreme as those at shorter (i.e., the CaH and TiO bands between 6600–7300 Å) or longer wavelengths (i.e., the strong H₂ absorption). The comparisons shown in Figure 3 indicate a spectral type of sdL3.5 for SDSS J1256–0224 on the Burgasser, Cruz & Kirkpatrick (2007) scheme. This is only 0.5 subtypes earlier than the sdL4 classification of 2MASS J1626+3925, consistent with both the overall similarities between the spectra of these two sources and slight differences in their atomic line and molecular band strengths.

3.2. Absolute Brightness and Distance

Parallax distance measurements have recently become available for low-temperature subdwarfs spanning types sdM7 to sdL7 (Monet et al. 1992; Dahn et al. 2008; Burgasser et al. 2008; Schilbach, Röser & Scholz 2009), including SDSS J1256–0224 for which Schilbach, Röser & Scholz (2009) determine $d = 90 \pm 23$ pc. This measurement is fairly uncertain, so we have compared it to the linear absolute magnitude/spectral type relations recently quantified by Cushing et al. (2009) for ultracool subdwarfs:

$$M_J = 8.02 + 0.313 \times \text{SpT} \quad (1)$$

$$M_H = 7.77 + 0.300 \times \text{SpT} \quad (2)$$

$$M_{K_s} = 7.44 + 0.320 \times \text{SpT} \quad (3)$$

where SpT(sdM7) = 7, SpT(sdL0) = 10, etc. These relations predict $M_J = 12.23 \pm 0.22$, $M_H = 11.81 \pm 0.23$ and $M_{K_s} = 11.75 \pm 0.25$ for a type of sdL3.5 \pm 0.5, and hence $d = 66 \pm 9$ pc for SDSS J1256–0224 based on the photometry of Schilbach, Röser & Scholz (2009) (the distance uncertainty includes contributions from photometry, a 0.5 subtype classification uncertainty, covariance matrix elements for the Cushing et al. 2009 relations, and variation in distance estimates between JHK_s values). This distance inferred estimate is considerably closer than the mean value from Schilbach, Röser & Scholz (2009) but nevertheless consistent within experimental uncertainties. It is also roughly half the 120 pc estimate of Burgasser, Cruz & Kirkpatrick (2007) and 50% larger than the 42 pc estimate of Sivarani et al. (2009). As the Cushing et al. (2009) relations provide the most accurate assessment of the ultracool subdwarf spectral type/absolute magnitude scale thus far, we use our estimated value from these relations for subsequent analysis.

3.3. Kinematics

The proper motion of SDSS J1256–0224 as measured by Schilbach, Röser & Scholz (2009), in conjunction with our estimated distance, yields a tangential velocity $V_{tan} = 186 \pm 26$ km s^{−1}, where the uncertainty is dominated by the distance estimate. Note that this value is again roughly half that estimated by Burgasser, Cruz & Kirkpatrick (2007) due to the reduction in the estimated distance. Nevertheless, this motion is still indicative of halo kinematics. A radial velocity

(V_r) for SDSS J1256–0224 was computed from its optical spectrum, by comparing the measured line centers of the atomic lines listed in Table 2 to vacuum wavelengths obtained from the National Institute of Standards and Technologies atomic line database¹⁰ (Ralchenko et al. 2008). A heliocentric Doppler shift of -130 ± 11 km s^{−1} was determined, which includes a barycentric motion correction of -15 km s^{−1}. The uncertainty in V_r includes the standard deviation in the line centers and a systematic uncertainty of 4 km s^{−1} based on the uncertainty of the wavelength dispersion solution. This value is nominally consistent with the -90 ± 40 km s^{−1} cross-correlation measurement of Sivarani et al. (2009); our improvement in precision is likely due to our higher signal-to-noise spectral data.

Adding in our radial velocity measurements, we find space velocities $[U, V, W] = [-115 \pm 11, -101 \pm 18, -150 \pm 9]$ km s^{−1} in the Local Standard of Rest (LSR), assuming an LSR solar motion of $[U, V, W]_{\odot} = [10, 5.25, 7.17]$ km s^{−1} (Dehnen & Binney 1998). Note that we adopt a right-handed velocity coordinate system with positive U pointing radially inward toward the Galactic center. The large space motions in all three LSR components are again strong indications of Galactic halo membership for SDSS J1256–0224.

3.4. Galactic Orbit

To explore the kinematics of SDSS J1256–0224 in more detail, we calculated its Galactic orbit using the inferred UVW velocities as initial conditions. These velocities were first converted to a Galactic inertial frame (assuming $V_{LSR} = +220$ km s^{−1}; Kerr & Lynden-Bell 1986), and the position and distance of SDSS J1256–0224 transformed to galactocentric rectangular coordinates $[X, Y, Z]$ aligned with $[U, V, W]$, assuming a Solar position of $[-8.5, 0, 0.027]$ kpc (Kerr & Lynden-Bell 1986; Chen et al. 2001). We adopt the convention of positive X pointing toward the Galactic center to align with our definition for U . The Galaxy was modeled using a set of static potentials comprising a spherically-symmetric halo and bulge and an axisymmetric, thin exponential disk. This model is a simplified version of the one described in Dehnen & Binney (1998) and includes the three density distributions:

$$\begin{aligned} \rho_{\text{bulge}}(r) &= \rho_{b0} \left(\frac{r}{a_b} \right)^{-\alpha_b} \\ \rho_{\text{halo}}(r) &= \rho_{h0} \left(\frac{r}{a_h} \right)^{-\alpha_h} \left(1 - \frac{r}{a_h} \right)^{\alpha_h - \beta_h} \\ \rho_{\text{disk}}(R, z) &= \Sigma_0 e^{-R/R_d} \delta(z) \end{aligned}$$

with spherical and polar coordinates $r \equiv \sqrt{X^2 + Y^2 + Z^2}$ and $R \equiv \sqrt{X^2 + Y^2}$. With these simplifications, the potentials corresponding to the bulge and halo densities can be expressed in terms of special functions, and the potential of the disk evaluated on a grid by numerical integration. The parameters $\rho_{b0}, a_b, \alpha_b, \rho_{h0}, a_h, \alpha_h, \beta_h, \Sigma_0, R_d$ were adopted as given for Models I and II in Table 2.3 of Binney & Tremaine (2008), which fit the measured rotation curve of the

¹⁰ <http://physics.nist.gov/asd3>

Galaxy but bracket the range of allowable disk/halo mass ratio in the Solar circle (Model I describes a Galaxy dominated by the disk mass at the solar circle, in Model II the halo mass dominates at the solar circle). The orbit of SDSS J1256–0224 was integrated using a second-order leapfrog method (kick-drift-kick) with a constant timestep of 1 kyr for a total simulation time of 1 Gyr centered on the present epoch. Energy was conserved to better than 1 part in 10^{-4} over the full length of the simulation, with the error dominated by the resolution of the grid on which the disk force and potential were interpolated. The Z component of angular momentum was conserved to 1 part in 10^{-13} .

Figure 4 displays the resulting orbit of SDSS J1256–0224 using Model I (Model II provides essentially identical results). The general character of this orbit is similar to several other ultracool subdwarfs, with a prograde eccentric orbit with apoaps near the Solar radius ($3.5 \lesssim R \lesssim 11$ kpc, $e = 0.5$) and substantial deviations from the Galactic plane ($Z_{\max} \approx \pm 7.5$ kpc). In terms of eccentricity, the orbit of SDSS J1256–0224 is more similar to that of 2MASS J0532+8246 ($e = 0.5$, $3 \lesssim R \lesssim 8.5$; Burgasser et al. 2008) and less ballistic than that of the sdM8 LSR 1425+7102 (Lépine, Shara, & Rich 2003) which plunges to within 1 kpc from the Galactic center (Dahn et al. 2008). The inclination of SDSS J1256–0224’s orbit, $\tan i \approx R_{\max}/Z_{\max}$, is quite a bit larger, nearly 45° with respect to the Galactic plane as compared to $\sim 15^\circ$ and $\sim 30^\circ$ for 2MASS J0532+8246 and LSR 1425+7102, respectively.

The orbital characteristics of SDSS J1256–0224, 2MASS J0532+8246 and LSR 1425+7102 are all consistent with membership in the Galaxy’s inner halo population (Chiba & Beers 2001; Carollo et al. 2007). The inner halo is believed to dominate the halo population in the inner 10–15 kpc of the Galaxy and has a typical metallicity of $[M/H] \sim -1.6$ (Carollo et al. 2007; see also Gizis 1997). Membership in the inner halo suggests an origin in the dissipative mergers of satellite galaxies (e.g., Searle & Zinn 1978; Chiba & Beers 2001; Bell et al. 2008). It is possible that the similarity of these orbits arise from selection effects. Stars spend a larger percentage of their orbital periods near apoaps (in this case near the Sun), and short, highly eccentric orbits would more frequently align with the Sun’s Galactic position. However, the recent discovery of the L subdwarf 2MASS J0616-6406, whose highly retrograde orbit extends out to $\gtrsim 30$ kpc making it a likely member of the Galaxy’s outer halo population (Cushing et al. 2009), suggests that ultracool subdwarfs may nevertheless be well-mixed in the vicinity of the Sun.

4. ATMOSPHERIC PROPERTIES

The distance and kinematics of SDSS J1256–0224 do not provide useful constraints on its atmospheric properties— T_{eff} , surface gravity ($\log g$) and metallicity ($[M/H]$). Such determinations require empirical calibrations (e.g., well-characterized coeval companions or cluster properties; Gizis & Reid 1997) or direct comparison to spectral models (e.g., Woolf & Wallerstein 2006). As SDSS J1256–0224 is a seemingly isolated source, we used the latter approach, employing the most recent generation of the COND-PHOENIX atmo-

sphere simulations (Hauschildt, Baron & Allard 1997; Hauschildt, Allard & Baron 1999; Baraffe et al. 2003) and the DRIFT-PHOENIX model atmospheres (Dehn 2007; Helling et al. 2008b; Witte 2008).

4.1. Spectral Models

PHOENIX is a general-purpose model atmosphere code, using plane-parallel geometry, thermochemical equilibrium calculations and opacity sampling to self-consistently solve for the temperature-pressure profile, chemical abundances and radiative/convective energy transfer through the atmosphere. Several implementations of PHOENIX have been used to study late-type dwarfs, incorporating various assumptions on elemental abundances, atomic and molecular opacities, line profiles, condensate formation and convective overshoot (e.g., Hauschildt, Allard & Baron 1999; Allard et al. 2001; Johnas et al. 2008; Helling et al. 2008b).

Here we examine two implementations of PHOENIX, the GAIA-COND models (Hauschildt et al. 2003) and the DRIFT models (Dehn 2007; Helling et al. 2008b; Witte 2008), which differ only in their treatment of the dust cloud layers. The former are most similar to the COND-PHOENIX model set developed by Allard et al. (2001), in which condensate species are treated as element sinks only and phase-equilibrium is assumed. Hence, COND-PHOENIX models simulate dust-free but element-depleted atmospheres. The DRIFT-PHOENIX models apply an advanced model of non-equilibrium grain formation, including seed formation, growth, evaporation, sedimentation and convective up-mixing to simulate the size distribution, abundances and vertical distribution of grains and their material composition (Woitke & Helling 2003, 2004; Helling & Woitke 2006; Helling, Woitke & Thi 2008). In this approach, each size-variable grain is made of a variety of compounds which changes with height according to its formation history. Alternate prescriptions for modeling condensate grain formation in cool dwarf atmospheres have been explored by Ackerman & Marley (2001); Allard et al. (2003); Cooper et al. (2003); Tsuji (2002, 2005); Tsuji, Nakajima & Yanagisawa (2004) and Burrows, Sudarsky & Hubeny (2006); a thorough comparison of these cloud models is given in Helling et al. (2008a).

For this study, we employed both GAIA COND-PHOENIX and DRIFT-PHOENIX atmosphere models spanning $2000 \leq T_{\text{eff}} \leq 3500$ K (steps of 100 K), $\log g = 5.0$ and 5.5 (cgs) and $-3.0 \leq [M/H] \leq 0.0$ (steps of 0.5 dex; Solar $[M/H] \equiv 0$). Elemental abundances are scaled from Anders & Grevesse (1989) and Grevesse, Noels & Sauval (1992).

4.2. Color Comparisons

We pursued a two-step comparison of SDSS J1256–0224 to the models, first examining optical/near-infrared colors $i' - J$ and $J - K_s$ (see also Scholz et al. 2004b; Dahn et al. 2008; Schilbach, Röser & Scholz 2009). Synthetic colors were computed directly from the model atmosphere spectra by convolving each with filter profiles from SDSS (Fukugita et al. 1996, on the AB magnitude system) and 2MASS (Cohen, Wheaton & Megeath 2003, on the

Vega magnitude system). The filter profiles include the effects of detector quantum efficiency, telescope throughput and atmospheric transmission, all of which are essential for the complex spectra of late-type dwarfs (e.g., Stephens & Leggett 2004).

Figure 5 displays colors for both model sets for $\log g = 5.5$ and the full range of T_{eff} and $[M/H]$. In addition to measurements for SDSS J1256–0224, we all show color data for five subdwarfs classified sdM8 and later: the sdM8 LSR 1425+7102, (Lépine, Shara, & Rich 2003); the sdM8.5 2MASS J01423153+0523285 (Burgasser, Cruz & Kirkpatrick 2007, hereafter 2MASS J0142+0523); SSSPM J1013-1356, 2MASS J1626+3925 and 2MASS J0532+8246. Near-infrared photometry for all sources are from 2MASS or Schilbach, Röser & Scholz (2009), with the exception of 2MASS J0142+0523 for which a synthetic $J - K_s$ color was calculated using near-infrared spectral data from Burgasser et al. (2004). SDSS i' magnitudes for SDSS J1256–0224 and 2MASS J1626+3925 are from SDSS DR6; for the other sources, i' magnitudes were bootstrapped from I_N photometry from the Super-Cosmos Sky Survey (SSS; Hambly et al. 2001a,b,c) by calculating synthetic $i' - I_N$ colors from published optical spectral data for these sources (Burgasser et al. 2003a; Lépine, Shara, & Rich 2003; Scholz et al. 2004b; Burgasser, Cruz & Kirkpatrick 2007). The uncertainties for the spectroscopy-based magnitudes were assumed to be 0.1 mag, based on prior work (e.g., Burgasser et al. 2002).

For the GAIA COND-PHOENIX models, predicted colors encompass the measured values of all the subdwarfs shown with the exception of 2MASS J0532+8246. Lower temperatures for a given metallicity generally yield redder $i' - J$ and bluer $J - K_s$ colors, except at for $[M/H] < -2.0$ for which $i' - J$ colors actually turn blue. Lower metallicities at a given T_{eff} lead to bluer $i' - J$ and $J - K_s$ colors. SDSS J1256–0224 and 2MASS J1626+3925 both fall along the $[M/H] = -1.0$ line in this diagram (as do LSR 1425+7102 and 2MASS J0142+0523) around $T_{\text{eff}} = 2300$ and 2150 K, respectively. For $\log g = 5.0$, colors for these sources agree with model atmosphere metallicities and temperatures ~ 0.2 dex and ~ 100 K lower, respectively. The inferred model parameters based on these colors must be treated with caution, however, as the $[M/H] = 0$ GAIA COND-PHOENIX models do not track well with mean $i' - J$ versus $J - K_s$ colors of M0–L0 field dwarfs as compiled by West et al. (2008). The divergence is likely due to absence of condensate opacity in the GAIA models, which are known to be necessary in reproducing the colors of late-type M and L dwarfs (e.g., Allard et al. 2001).

The DRIFT-PHOENIX models exhibit very different color trends below $T_{\text{eff}} \approx 2500$ K as condensates become a prominent opacity source in the photosphere. both $i' - J$ and $J - K_s$ colors trend redder for lower T_{eff} for $[M/H] > -2.5$, with a notable kink in color tracks at $T_{\text{eff}} \approx 2200$ –2300 not present in the GAIA COND-PHOENIX models. The additional reddening places the $[M/H] = 0$ models into closer agreement with the mean colors of L0 dwarfs, although they still diverge from M5–M9 dwarfs. The $J - K_s$ color reversal affects all metallicities, with the result that none of the models reproduce the measured colors of the L subdwarfs SDSS J1256–0224,

2MASS J1626+3925 and 2MASS J0532+8246 ($\log g = 5.0$ models show similar behavior). The deviation of the models away from the measured photometry is likely due to the model i -band magnitudes, which are highly sensitive to the strong molecular opacity present at these wavelengths (see § 4.3). A rough extrapolation of the models suggests lower metallicities for SDSS J1256–0224 and 2MASS J1626+3925, $[M/H] \sim -2.0$ to -1.5 .

4.3. Spectral Comparisons

To further assess the agreement between models with observations, we compared the observed spectrum of SDSS J1256–0224 directly to the GAIA COND-PHOENIX and DRIFT-PHOENIX model spectra for the same range of parameters shown in Figure 5. These comparisons were made to the combined red optical and near-infrared spectrum, which was stitched together by first smoothing the individual spectra to a common resolution of $\lambda/\Delta\lambda = 100$, scaling the spectra to match flux densities in the 0.8–0.9 μm range, and then combining the red optical spectral data for $\lambda < 0.9 \mu\text{m}$ with the near-infrared data for $\lambda > 0.9 \mu\text{m}$ ¹¹ (see Figure 2). The uncertainty spectrum (flux uncertainty as a function of wavelength) was combined using the same scaling factors and wavelength cutoffs. We then interpolated the entire spectrum onto a linear wavelength scale (note that a wavelength scale uniform in frequency produced similar results).

Observational and model spectra were initially normalized over the 0.9–1.0 μm range; then, for each model spectrum, a goodness-of-fit statistic was calculated,

$$\Gamma_{\{p\}} = \sum_{\{\lambda\}} W(\lambda) \frac{[F(\lambda) - \alpha S_{\{p\}}(\lambda)]^2}{\alpha S_{\{p\}}(\lambda) \sigma(\lambda)}. \quad (4)$$

Here, $F(\lambda)$ and $\sigma(\lambda)$ are the observed spectrum and uncertainty; $S_{\{p\}}(\lambda)$ is the model spectrum for model parameters $\{p\} = \{T_{\text{eff}}, \log g, [M/H]\}$; α is a normalization scale factor for the model spectrum; and $W(\lambda)$ is a weighting function that satisfies $\sum_{\{\lambda\}} W(\lambda) = 1$. This form was chosen as a compromise between a standard χ^2 formulation (e.g., $\sum [F - S]^2/S$) and a reduced χ^2 formulation (e.g., $\sum [F - S]^2/\sigma^2$), as the former places too much emphasis on the lowest signal regions (i.e., strong absorption features) while the latter places too much emphasis on the highest signal-to-noise continuum regions (e.g., the 0.9–1.1 μm peak). For alternate approaches, see Takeda (1995) and Cushing et al. (2008). The sums were computed over the spectral range $\{\lambda\} = 0.64$ –2.4 μm . The normalization factor α was allowed to vary over 0.5–1.5 to account for continuum offsets between the observed and model spectra, and the normalization with the minimum Γ was retained. Various weighting functions $W(\lambda)$ were considered, but ultimately we settled on one that was constant for all wavelengths.¹² Note that we do not consider Γ a robust estimator; it merely provides a quantitative measure of the best-fit model to the data. The

¹¹ Red optical data were only used up to 0.9 μm due to concerns over the relative flux calibration of these data over the 0.9–1.0 μm range; see discussion in Burgasser, Cruz & Kirkpatrick (2007).

¹² Cushing et al. (2008), in their analysis of optical and infrared spectra of late-type dwarfs, considered a weighting function that scaled with the width of each spectral wavelength bin. As we interpolate the observed and model spectra onto a common, linear wavelength scale, our constant weighting scheme is equivalent.

best fits (minimum Γ) were also visually compared to verify that they did indeed provide a good match to the data.

Table 3 lists the parameters for the five best fits for the GAIA COND-PHOENIX and DRIFT-PHOENIX models; the single best-fit models are compared with the data in Figure 6. The best-fit model parameters are similar between the two sets, with $T_{eff} = 2300$ –2500 K and $[M/H] = -1.5$ to -1.0 for the GAIA COND-PHOENIX models, and $T_{eff} = 2100$ –2400 K and $[M/H] = -1.5$ and for the DRIFT-PHOENIX models. These parameters includes models with $\log g = 5.0$ and 5.5 ; lower gravities are generally matched with lower metallicities, which may simply indicate a tradeoff in the inferred photospheric pressure ($P_{ph} \propto g/\kappa$, where κ is the Rosseland mean opacity which is generally smaller for lower metallicities). A higher surface gravity is in fact preferred if this object is a low-mass member of the halo population as evolutionary models predict that a 5 Gyr source with $T_{eff} = 2100$ –2500 K should have $\log g = 5.3$ – 5.5 and mass 0.08 – $0.085 M_{\odot}$ (Burrows et al. 2001; Baraffe et al. 2003). Indeed, there are more best-fitting models with $\log g = 5.5$ than 5.0.

Encouragingly, the best-fit parameters for both GAIA COND-PHOENIX and DRIFT-PHOENIX models are similar to the best-fit parameters from the GAIA COND-PHOENIX color comparison. The metallicities inferred from both color and spectral comparisons are also consistent with the mean metallicities of inner halo stars (Carollo et al. 2007). In addition, we find that both sets of models do a reasonably good job at matching the overall spectral energy distribution of SDSS J1256–0224, in particular fitting the blue spectral slope from 1.3 – $2.4 \mu\text{m}$ and the depth of the 1.4 and $1.9 \mu\text{m}$ H_2O bands. The GAIA COND-PHOENIX models also provide a fairly good match to the 0.9 – $1.3 \mu\text{m}$ spectral peak, reproducing the strong FeH bands at 0.99 and $1.25 \mu\text{m}$ but predicting excessively strong alkali lines in this region. The DRIFT-PHOENIX models do a poorer job in this region, failing to reproduce the $1.1 \mu\text{m}$ spectral peak and, like the GAIA COND-PHOENIX models, exhibiting excessively strong alkali lines.

There are more significant deficiencies in the red optical region, however, with both model sets failing to reproduce spectral features in detail, particularly around the spectral peaks at 6600 and 7400 \AA . The models predict excessively strong Rb I and Na I alkali lines, and appear to be missing CrH and FeH opacity in the 8600 – 8700 \AA region. The DRIFT-PHOENIX models exhibit excessively strong TiO absorption at 8400 \AA , and pronounced discrepancies in the 6700 \AA CaH and 7200 \AA TiO bands. Surprisingly, the older GAIA COND-PHOENIX models provide overall better fits to the red optical data, although there are still clear problems in alkali line strengths, excessive emission in the pseudo-continua between 6000 – 7500 \AA , and missing CrH and FeH opacity. These discrepancies, which influence model $i' - J$ color trends (Figure 5) are probably attributable in part to inadequate treatment of the far-wing line profiles of the pressure-broadened Na I and K I doublets, as more recent opacity calculations have not incorporated in the present models (Burrows & Volobuyev 2003; Johnas et al. 2008). The treatment of dust formation

can influence these line profiles due to feedback on the temperature structure (Johnas et al. 2008). It is therefore promising that the K I line cores and other alkali line strengths are reproduced better in the DRIFT-PHOENIX models. Incompleteness in molecular opacities (e.g., TiO, CrH and FeH) are also likely responsible, a well-known problem in modeling the optical spectra of normal L dwarfs (e.g., Kirkpatrick et al. 1999a). We cannot rule out the additional influence of elemental composition variations, which are present in subsolar metallicity stars (e.g., Edvardsson et al. 1993; Fulbright 2000; Asplund et al. 2006) and can influence the overall atmospheric chemical pathways. The red optical region clearly remains problematic for low-temperature model atmospheres regardless of metallicity (see also Burgasser, Cruz & Kirkpatrick 2007), although the incorporation of condensate dust formation appears to be aiding alkali line fits somewhat.

4.4. Discussion

While it appears that the inclusion of condensate grain formation as specified by the DRIFT-PHOENIX models provides some improvement to the near-infrared colors and alkali line profiles of ultracool dwarfs and subdwarfs, the overall better spectral and color fits to SDSS J1256–0224 by the condensate-free GAIA COND-PHOENIX models suggests that grain chemistry may be unimportant in metal-poor atmospheres. This has been the conclusion of several studies, citing the presence of enhanced metal-oxide bands, strong lines from refractory species, and blue near-infrared colors as consistent with largely condensate-free photospheres (Burgasser et al. 2003a; Gizis & Harvin 2006; Reiners & Basri 2006; Burgasser, Cruz & Kirkpatrick 2007).

However, there are problems with this simple interpretation. It is clear that TiO and VO features weaken from the M subdwarfs to the L subdwarfs, and continue to weaken even through the current L subdwarf sequence (e.g., Burgasser, Cruz & Kirkpatrick 2007). This trend is consistent with the depletion of refractory gas-phase elements with decreasing temperature. In contrast, TiO and VO bands are stronger in later-type M giants where low atmospheric pressure inhibits condensation (see Lodders 2002). Conclusions that gaseous TiO and VO bands are nevertheless enhanced may also be biased by simple equilibrium treatments of condensation chemistry. Helling, Woitke & Thi (2008) have shown that rare-element compounds, including Ca- and Ti-bearing condensates, never achieve phase-equilibrium in low-temperature atmospheres; hence, the abundances of gas molecules are generally higher in non-equilibrium cloud models such as DRIFT-PHOENIX. The fact that the metal-oxide bands observed in the spectrum of SDSS J1256–0224 are actually *weaker* than predicted by the best-fit DRIFT-PHOENIX cloud models suggests that condensate grain formation may actually be *more efficient* in metal-poor atmospheres than these models predict. There are some important caveats to this interpretation, however. Incomplete molecular and pressure-broadened line opacities are clearly an issue for low-temperature atmospheres, affecting in particular pressure-temperature profiles and associated chemistry through the photosphere. Also, we have only examined one prescription of grain formation in this study; cur-

rent cloud models have not yet reached agreement (e.g., Helling et al. 2008a). It is clear that conclusive statements on the efficiency of condensation in metal-poor atmospheres are premature; models are simply not yet adequate to address this question.

Another consideration, independent of the state of current model atmospheres, is the possibility that L subdwarfs are simply warmer than equivalently-classified L dwarfs. The T_{eff} inferred for SDSS J1256–0224, roughly in the range 2100–2500 K, is comparable to those for solar-metallicity L0–L2 dwarfs (e.g., Vrba et al. 2004). At these temperatures, condensates play a less prominent role in atmospheric opacity than for cooler/late-type dwarfs. Similarly, the sdL7 2MASS J0532+8246 has been shown to have a $T_{eff} = 1730 \pm 90$ K, comparable to L4–L5 dwarfs. This shift is due in large part to the classification methodology proposed by Burgasser, Cruz & Kirkpatrick (2007). Comparison of L dwarf and subdwarf optical spectra in the 7300–9000 Å range emphasizes the importance of the pressure-broadened 7700 Å K I doublet. This feature is inherently pressure-sensitive, and at a given temperature will be deeper and broader in the higher-pressure, metal-poor (small κ) photospheres of L subdwarfs. As such, the apparent persistence of TiO absorption in L subdwarfs may simply reflect a shift in temperature scale and not condensation abnormalities (see also Burgasser & Kirkpatrick 2006).

Such shifts in inferred quantities like temperature and metallicity have been seen as an inherent weakness in the classification scheme of ultracool subdwarfs in general (e.g., Jao et al. (2008)). However, the current state of flux in theoretical models should also emphasize the importance of divorcing classification (a purely empirical exercise) from interpretive physical parameters. The former is built upon a set of specific standard stars, not models, although standards are as yet in insufficient supply for the L subdwarfs. As more examples are uncovered, measurement of their luminosities and T_{eff} s, and improved theoretical modeling particularly of optical spectra, will provide necessary the constraints to calibrate a future classification sequence and enable more robust assessment on condensate grain formation efficiency that is currently possible.

5. SUMMARY

We have presented a thorough analysis of the red optical and near-infrared spectrum of the L subdwarf SDSS J1256–0224, originally identified by Sivarani et al. (2009) in the SDSS survey. This source is similar to the sdL4 2MASS J1626+3925 at both optical and near-infrared wavelengths, and we determine an sdL3.5 classification following the preliminary scheme of Burgasser, Cruz & Kirkpatrick (2007). Using the absolute magnitude/spectral type relations for ultracool subdwarfs recently defined by Cushing et al. (2009), we esti-

mate a distance of 66 ± 9 pc to this source, formally consistent with the less precise 90 ± 23 pc parallax distance measurement made by Schilbach, Röser & Scholz (2009). Combined with its high proper motion and radial velocity, we confirm that SDSS J1256–0224 is a kinematic member of the Galactic inner halo, with a modestly eccentric and highly inclined Galactic orbit whose apoaps is near the Sun. A comparison of the colors and spectra of SDSS J1256–0224 to GAIA COND-PHOENIX and DRIFT-PHOENIX atmospheric models indicate best-fit atmospheric parameters of $T_{eff} = 2100\text{--}2500$ K and $[M/H] = -1.5$ to -1.0 for $\log g = 5.0\text{--}5.5$, although discrepancies between the models and the data, particularly in the red optical region, indicate that these parameters be treated with caution. Comparisons to the DRIFT-PHOENIX models contradict prior conclusions that condensate formation may be inhibited in metal-poor, low-temperature atmospheres. Non-equilibrium grain species abundances (particularly for Ti- and Ca-bearing species) predict even stronger metal-oxide bands than those observed in the spectrum of SDSS J1256–0224, and thus enhanced condensate formation in the atmosphere of this metal-poor source. Improvements to the model atmospheres in the red optical region are necessary before any conclusive statement can be made. In addition, the possibility that the temperature scale of L subdwarfs is warmer than that of L dwarfs may provide a sufficient explanation for strong metal-oxide bands irrespective of grain chemistry.

The authors would like to thank telescope operators Dave Griep and Mauricio Martinez, and instrument specialists John Rayner and Jorge Bravo for their assistance during the IRTF and Magellan observations. AJB thanks J. Bochanski and A. West for useful discussion on Galactic coordinate systems. SW acknowledges the Graduierten Kollege 1351 from the German Research Council. This publication makes use of data from the Two Micron All Sky Survey, which is a joint project of the University of Massachusetts and the Infrared Processing and Analysis Center, and funded by the National Aeronautics and Space Administration and the National Science Foundation. 2MASS data were obtained from the NASA/IPAC Infrared Science Archive, which is operated by the Jet Propulsion Laboratory, California Institute of Technology, under contract with the National Aeronautics and Space Administration. Based on observations obtained 6.5 meter Magellan Telescopes located at Las Campanas Observatory, Chile. The authors wish to recognize and acknowledge the very significant cultural role and reverence that the summit of Mauna Kea has always had within the indigenous Hawaiian community. We are most fortunate to have the opportunity to conduct observations from this mountain.

Facilities: IRTF (SpeX), Magellan Clay (LDSS-3)

REFERENCES

- Abell, G. O. 1959, *PASP*, 67, 258
- Ackerman, A. S., & Marley, M. S. 2001, *ApJ*, 556, 872
- Adelman-McCarthy, J. K., et al. 2008, *ApJS*, 175, 297
- Allard, F., Guillot, T., Ludwig, H.-G., Hauschildt, P. H., Schweitzer, A., Alexander, D. R., & Ferguson, J. 2003 in *Brown Dwarfs*, Proceedings of IAU Symposium 211, ed. E. Martín (San Francisco: ASP), p. 32
- Allard, F., Hauschildt, P. H., Alexander, D. R., Tamanai, A., & Schweitzer, A. 2001, *ApJ*, 556, 357

- Allington-Smith, J., et al. 1994, *PASP*, 106, 983
- Anders, E., & Grevesse, N. 1989, *Geochim. Cosmochim. Acta*, 53, 197
- Asplund, M., Lambert, D. L., Nissen, P. E., Primas, F., & Smith, V. V. 2006, *ApJ*, 644, 229
- Baraffe, I., Chabrier, G., Barman, T., Allard, F., & Hauschildt, P. H. 2003, *A&A*, 402, 701
- Bell, E. F., et al. 2008, *ApJ*, 680, 295
- Benjamin, R. A., et al. 2005, *ApJ*, 630, L149
- Binney, J., & Tremaine, S. 2008, *Galactic Dynamics*, Princeton Series in Astrophysics, Princeton University Press, 2nd edition
- Borysow, A., Jørgensen, U. G., & Zheng, C. 1997, *A&A*, 324, 185
- Burgasser, A. J. 2004 *ApJ*, 614, L73
- Burgasser, A. J., Cruz, K. L., & Kirkpatrick, J. D. 2007, *ApJ*, 657, 494
- Burgasser, A. J., & Kirkpatrick, J. D. 2006, *ApJ*, 645, 1485
- Burgasser, A. J., Kirkpatrick, J. D., & Burrows, A. 2006, *ApJ*, 639, 1095
- Burgasser, A. J., Kirkpatrick, J. D., Burrows, A., Liebert, J., Reid, I. N., Gizis, J. E., McGovern, M. R., Prato, L., & McLean, I. S. 2003a, *ApJ*, 592, 1186
- Burgasser, A. J., Kirkpatrick, J. D., & Lépine, S. 2005 in *The 13th Cambridge Workshop on Cool Stars, Stellar Systems, and the Sun (ESA-SP-560)*, ed. F. Favata, G. A. J. Hussain & B. Battrock (Noordwijk: ESA), p. 237
- Burgasser, A. J., McElwain, M. W., Kirkpatrick, J. D., Cruz, K. L., Tinney, C. G., & Reid, I. N. 2004 *AJ*, 127, 2856
- Burgasser, A. J., Vrba, F. J., Lépine, S., Munn, J. A., Luginbuhl, C. B., Henden, A. A., Guetter, H. H., & Canzian, B. C. 2008, *ApJ*, 672, 1159
- Burgasser, A. J., et al. 2002, *ApJ*, 564, 421
- Burrows, A., Hubbard, W. B., Lunine, J. I., & Liebert, J. 2001, *Rev. of Modern Physics*, 73, 719
- Burrows, A., Hubbard, W. B., Saumon, D., & Lunine, J. I. 1993, *ApJ*, 406, 158
- Burrows, A., & Sharp, C. M. 1999, *ApJ*, 512, 843
- Burrows, A., Sudarsky, D., & Hubeny, I. 2006, *ApJ*, 640, 1063
- Burrows, A., & Volobuyev, M. 2003, *ApJ*, 583, 985
- Carollo, D., et al. 2007, *Nature*, 450, 1020
- Chiba, M., & Beers, T. C. 2001, *ApJ*, 549, 325
- Chen, B., et al. 2001, *ApJ*, 553, 184
- Cohen, M., Wheaton, W. A., & Megeath, S. T. 2003, *AJ*, 126, 1090
- Cooper, C. S., Sudarsky, D., Milsom, J. A., Lunine, J. I., & Burrows, A. 2003, *ApJ*, 586, 1320
- Chiu, K., Fan, X., Leggett, S. K., Golimowski, D. A., Zheng, W., Geballe, T. R., Schneider, D. P., & Brinkmann, J. 2006, *AJ*, 131, 2722
- Cruz, K. L., Reid, I. N., Liebert, J., Kirkpatrick, J. D., & Lowrance, P. J. 2003, *AJ*, 126, 2421
- Cushing, M. C., Looper, D., Burgasser, A. J., Kirkpatrick, J. D., Faherty, J., Cruz, K. L., & Sweet, A. 2009, *ApJ*, submitted
- Cushing, M. C., Marley, M. S., Saumon, D., Kelly, B. C., Vacca, W. D., Rayner, J. T., Freedman, R. S., Lodder, K., & Roellig, T. 2008, *ApJ*, 678, 1372
- Cushing, M. C., & Vacca, W. D. 2006, *AJ*, 131, 1797
- Cushing, M. C., Vacca, W. D., & Rayner, J. T. 2004, *PASP*, 116, 362
- Dahn, C. C., et al. 2002, *AJ*, 124, 1170
- Dahn, C. C., et al. 2008, *ApJ*, in press
- Dauphole, B., & Colin, J. 1995, *A&A*, 300, 117
- Dehn, M. 2007, Ph.D. Thesis, University Hamburg, Germany
- Dehnen, W., & Binney, J. J. 1998, *MNRAS*, 298, 387
- Edvardsson, B., Andersen, J., Gustafsson, B., Lambert, D. L., Nissen, P. E., & Tomkin, J. 1993, *A&A*, 275, 101
- Epchtein, N., et al. 1997, *The Messenger*, 87, 27
- Faherty, J. K., Burgasser, A. J., Cruz, K. L., Shara, M. M., Walter, F. M., & Gelino, C. R., 2008, *AJ*, in press
- Fukugita, M., Ichikawa, T., Gunn, J. E., Doi, M., Shimasaku, K., & Schneider, D. P. 1996, *AJ*, 111, 1748
- Fulbright, J. P. 2000, *AJ*, 120, 1841
- Geballe, T. R., et al. 2002, *ApJ*, 564, 466
- Gizis, J. E. 1997, *AJ*, 113, 806
- Gizis, J. E., & Harvin, J. 2006, *AJ*, 132, 2372
- Gizis, J. E., & Reid, I. N. 1997, *PASP*, 109, 849
- Grevesse, N., Noels, A., & Sauval, A. J. 1992, in *Coronal Streamers, Coronal Loops, and Coronal and Solar Wind Composition*, ed. C. Mattock (ESA SP-348; Noordwijk: ESA), 305
- Hambly, N. C., Davenhall, A. C., Irwin, M. J., & MacGillivray, H. T. 2001a, *MNRAS*, 326, 1315
- Hambly, N. C., Irwin, M. J., & MacGillivray, H. T. 2001b, *MNRAS*, 326, 1295
- Hambly, N. C., MacGillivray, H. T., Read, M. A., et al. 2001c, *MNRAS*, 326, 1279
- Hamuy, M., Suntzeff, N. B., Heathcote, S. R., Walker, A. R., Gigoux, P., & Phillips, M. M. 1994, *PASP*, 106, 566
- Hauschildt, P. H., Allard, F., & Baron, E. 1999, *ApJ*, 512, 377
- Hauschildt, P. H., Allard, F., Baron, E., Aufdenberg, J., & Schweitzer, A. 2003, in *GAIA Spectroscopy: Science and Technology (ASP Conf. Proc. 298)*, ed. U. Munari (ASP), p. 179
- Hauschildt, P. H., Baron, E., & Allard, F. 1997, *ApJ*, 483, 390
- Helling, Ch., et al. 2008, *MNRAS*, 391, 1854
- Helling, Ch., & Woitke, P. 2006, *A&A*, 455, 325
- Helling, Ch., Woitke, P., & Thi, W.-F. 2008, *A&A*, 485, 547
- Helling, Ch., Dehn, M., Woitke, P., & Hauschildt, P. H. 2008, *ApJ*, 675, L105
- Høg, E., Fabricius, C., Makarov, V. V., Urban, S., Corbin, T., Wycoff, G., Bastian, U., Schwekendiek, P., & Wicenec, A. 2000, *A&A*, 355, L27
- Hook, I., Jørgensen, I., Allington-Smith, J. R., Davies, R. L., Metcalfe, N., Murowinski, R. G., & Crampton, D. 2004, *PASP*, 116, 425
- Jao, W.-C., Henry, T. J., Beaulieu, T. D., & Subasavage, J. P. 2008, *AJ*, 136, 840
- Johnas, C. M. S., Helling, Ch., Dehn, M., Woitke, P., & Hauschildt, P. H. 2008, *MNRAS*, 385, L120
- Kerr, F. J., & Lynden-Bell, D. 1986, *MNRAS*, 221, 1023
- Kirkpatrick, J. D. 2005, *ARA&A*, 43, 195
- Kirkpatrick, J. D., Reid, I. N., Liebert, J., Gizis, J. E., Burgasser, A. J., Monet, D. G., Dahn, C. C., Nelson, B., & Williams, R. J. 2000, *AJ*, 120, 447
- Kirkpatrick, J. D., Allard, F., Bida, T., Zuckerman, B., Becklin, E. E., Chabrier, G., & Baraffe, I. 1999a, *ApJ*, 519, 834
- Kirkpatrick, J. D., et al. 1999b, *ApJ*, 519, 802
- Leggett, S. K., Allard, F., Dahn, C., Hauschildt, P. H., Kerr, T. H., & Rayner, J. 2000, *ApJ*, 535, 965
- Lépine, S., Rich, R. M., & Shara, M. M. 2003b, *ApJ*, 591, L49
- Lépine, S., Shara, M. M., & Rich, R. M. 2003, *ApJ*, 585, L69
- Lépine, S., Shara, M. M., & Rich, R. M. 2004, *ApJ*, 602, L125
- Liebert, J., & Probst, R. G. 1987, *ARA&A*, 25, 473
- Linsky, J. L. 1969, *ApJ*, 156, 989
- Lodders, K. 2002, *ApJ*, 577, 974
- Miyamoto, M., & Nagai, R. 1975, *PASJ*, 27, 533
- Monet, D. G., Dahn, C. C., Vrba, F. J., Harris, H. C., Pier, J. R., Luginbuhl, C. B., & Ables, H. D. 1992, *AJ*, 103, 638
- Mould, J. R., & Hyland, A. R. 1976, *ApJ*, 208, 399
- Oke, J. B., et al. 1995, *PASP*, 107, 375
- Patten, B. M., et al. 2006, *ApJ*, 651, 502
- Pier, J. R., Munn, J. A., Hindsley, R. B., Hennessy, G. S., Kent, S. M., Lupton, R. H., & Ivezić, Ž. 2003, *AJ*, 125, 1559
- Ralchenko, Yu., Kramida, A. E., Reader, J., and NIST ASD Team. 2008, NIST Atomic Spectra Database (version 3.1.5), <http://physics.nist.gov/asd3>
- Rayner, J. T., Toomey, D. W., Onaka, P. M., Denault, A. J., Stahlberger, W. E., Vacca, W. D., Cushing, M. C., & Wang, S. 2003, *PASP*, 155, 362
- Reid, I. N., et al. 1991, *PASP*, 103, 661
- Reiners, A., & Basri, G. 2006, *AJ*, 131, 1806
- Richer, H. B., et al. 2008, *AJ*, 135, 2141
- Saumon, D., Bergeron, P., Lunine, J. I., Hubbard, W. B., & Burrows, A. 1994, *ApJ*, 424, 333
- Schmilbach, E., Röser, S., & Scholz, R.-D. 2009, *A&A*, in press
- Schmidt, S. J., Cruz, K. L., Bongiorno, B. J., Liebert, J., Reid, I. N. 2007, *AJ*, 133, 2258
- Scholz, R.-D., Lehmann, I., Matute, I., & Zinnecker, H. 2004, *A&A*, 425, 519
- Scholz, R.-D., Lodieu, J., & McCaughrean, M. 2004, *A&A*, 428, L25

- Scholz, R.-D., Storm, J., Knapp, G. R., & Zinnecker, H. 2009, A&A, in press
- Schuller, F., et al. 2003, A&A, 403, 955
- Searle, L. & Zinn, R. 1978, ApJ, 225, 357
- Sivarani, T., Lepine, S., Kembhavi, A. K., & Gupchup, J. 2009, ApJ, in press
- Skrutskie, M. F., et al. 2006, AJ, 131, 1163
- Stephens, D. C., & Leggett, S. K. 2004, PASP, 116, 9
- Takeda, Y. 1995, PASJ, 47, 287
- Tody, D. 1986, Proc. SPIE, 627, 733
- Tsuji, T. 2002, ApJ, 575, 264
- Tsuji, T. 2005, ApJ, 621, 1033
- Tsuji, T., Nakajima, R., & Yanagisawa, K. 2004, ApJ, 607, 511
- Tsuji, T., Ohnaka, K., & Aoki, W. 1996, A&A, 305, L1
- Vacca, W. D., Cushing, M. C., & Rayner, J. T. 2003, PASP, 155, 389
- Vrba, F. J., et al. 2004, AJ, 127, 2948
- West, A. A., Hawley, S. L., Bochanski, J. J., Covey, K. R., Reid, I. N., Dhital, S., Hilton, E. J., & Masuda, M. 2008, AJ, 135, 785
- Witte, S. 2008, Diploma Thesis, University of Hamburg, Germany
- Woolf, V. M., & Wallerstein, G. 2006, PASP, 118, 218
- Woitke, P., & Helling, Ch. 2003, A&A, 339, 297
- Woitke, P., & Helling, Ch. 2004, A&A, 414, 335
- York, D. G., et al. 2000, AJ, 120, 1579
- Zacharias, N., et al. 2000, AJ, 120, 2131

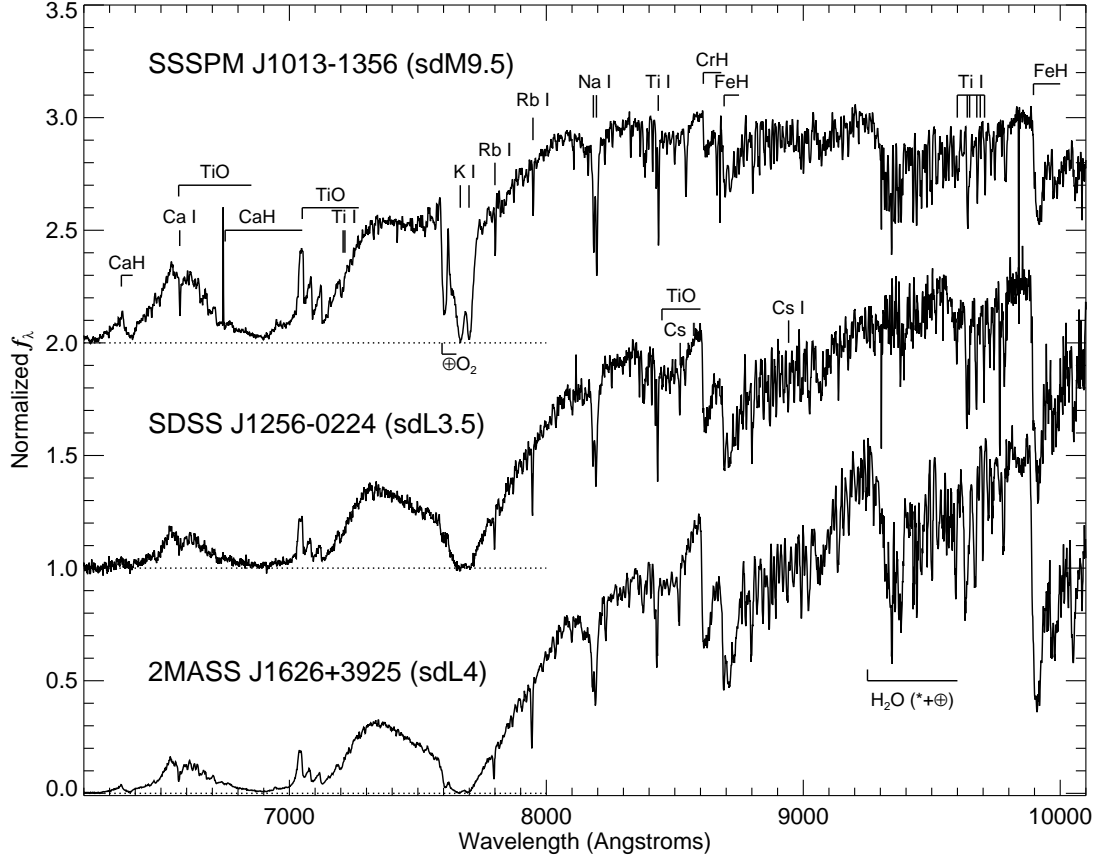


FIG. 1.— Red optical spectra of the SSSPM J1013-1356 (top), SDSS J1256-0224 (middle) and 2MASS J1626+3925 (bottom). Spectra are normalized in the 8500–8600 Å region and offset for comparison (dotted lines). Primary spectral features are indicated, as well as regions of strong telluric absorption (\oplus) in the spectra of SSSPM J1013-1356 and 2MASS J1626+3925.

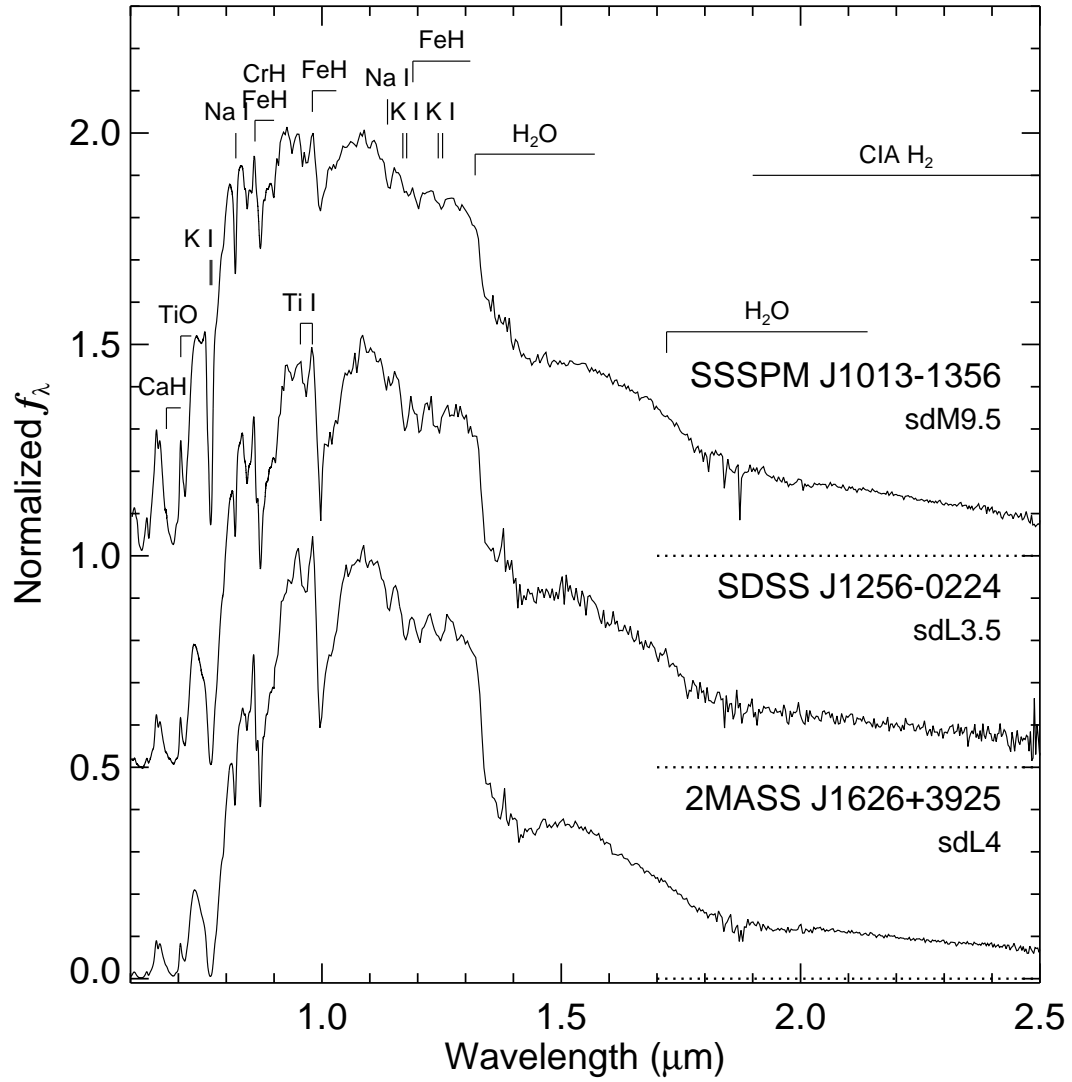


FIG. 2.— Low resolution near-infrared spectra of SSSPM J1013-1356 (top), SDSS J1256-0224 (middle) and 2MASS J1626+3925 (bottom), all obtained with SpeX in prism mode. Joined to these are the optical data from Figure 1, smoothed to the same resolution ($\lambda/\Delta\lambda \sim 120$). Spectra are normalized in the 0.9–1.0 μm region and offset for comparison (dotted lines). Primary spectral features are indicated.

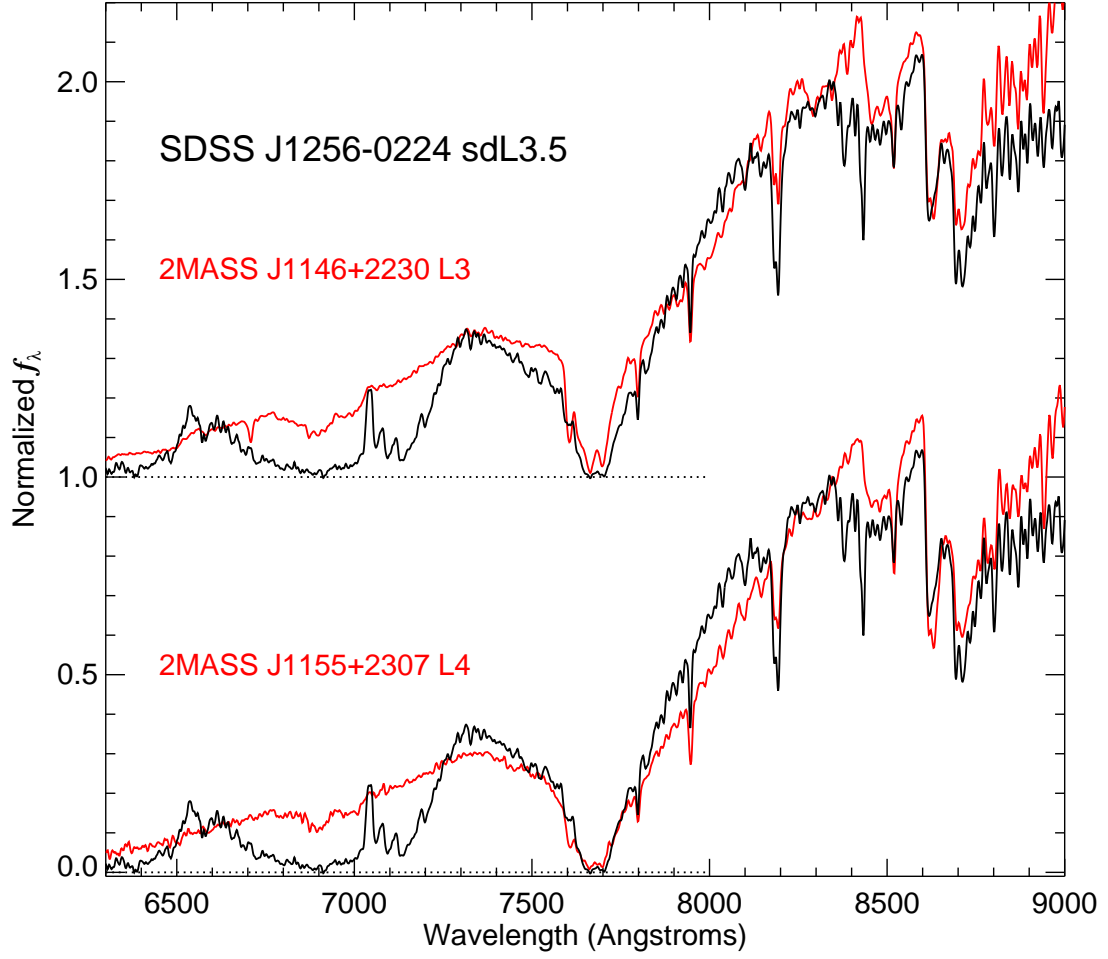


FIG. 3.— Optical spectrum of SDSS J1256–0224 (black lines) compared to the L dwarf optical standards (red lines) 2MASS J1146+2230 (L3) and 2MASS J1155+2307 (L4). All spectra are normalized in the 8250–8350 Å and offset for clarity (dotted lines). In the 7300–9000 Å range, the spectral morphology of SDSS J1256–0224 is intermediate between the two standards, indicating an sdL3.5 spectral type for this source based on the scheme of Burgasser, Cruz & Kirkpatrick (2007).

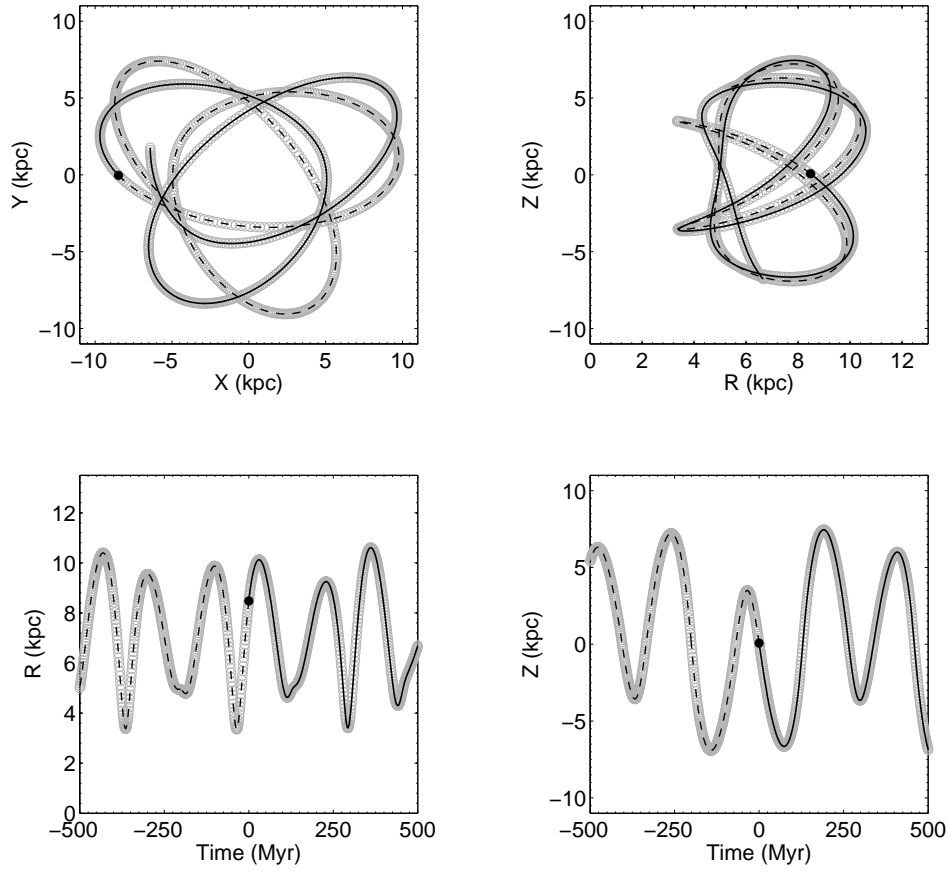


FIG. 4.— Galactic orbit of SDSS J1256–0224 over 1 Gyr centered on the current epoch, based on Galactic Model I from Binney & Tremaine (2008). Upper left and right panels shows orbit in $[X, Y]$ and $[R, Z]$ inertial frame coordinates; the current position of the Sun ($X_{\odot} = -8.5$ kpc, $Z_{\odot} = +27$ pc; Kerr & Lynden-Bell 1986; Chen et al. 2001) is indicated by the \odot symbol. Bottom panels show time evolution of R and Z . In all panels, past motion is indicated by dashed lines, future motion by solid lines, and current position by the black point.

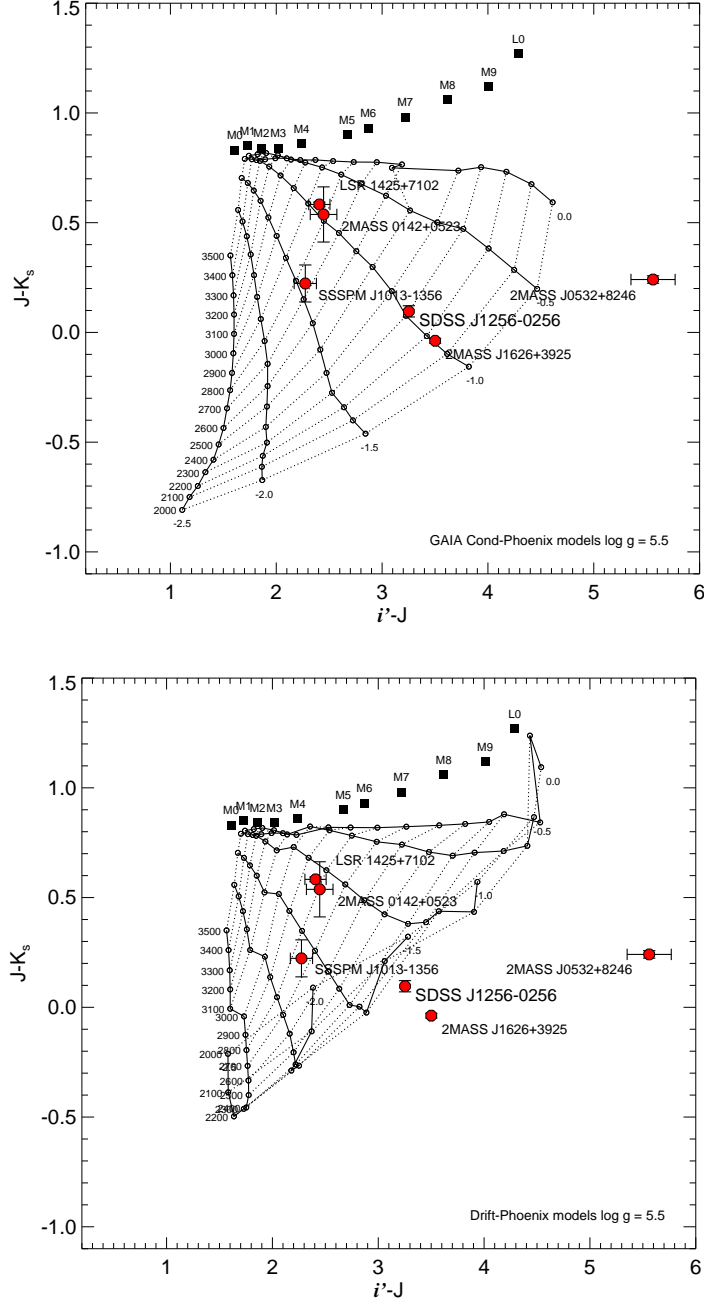


FIG. 5.— SDSS-2MASS $i' - J$ versus $J - K_s$ colors for the late-type subdwarfs 2MASS J0142+0523, LSR 1424+7102, SSSPM J1013-1356, SDSS J1256-0224, 2MASS J1626+3925 and 2MASS J0532+8246 as compared to GAIA COND-PHOENIX (top) and DRIFT-PHOENIX (bottom) atmospheric model predictions. Models are shown for $\log g = 5.5$, $2000 \leq T_{\text{eff}} \leq 3500$ K in steps of 100 K (along solid lines) and $-3.0 \leq [M/H] \leq 0$ in steps of 0.5 dex (along dotted lines). Also shown are mean SDSS-2MASS colors of M0-L0 dwarfs from West et al. (2008).

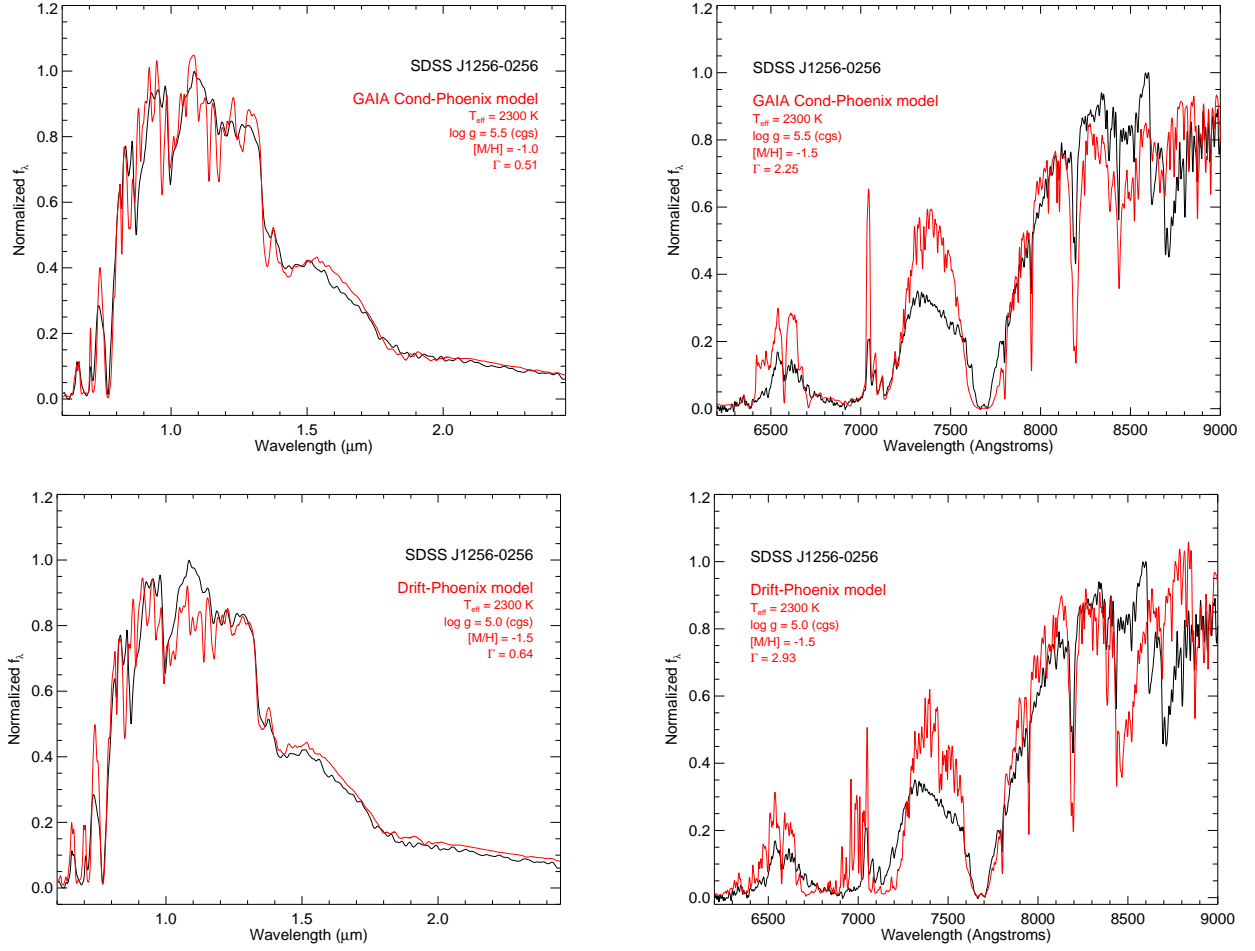


FIG. 6.— (Left) Best-fit GAIA COND-PHOENIX (top) and DRIFT-PHOENIX models (bottom; red lines) compared with the combined red optical and near-infrared spectrum of SDSS J1256–0224 (black lines). Both models and spectra have been smoothed to a resolution $\lambda/\Delta\lambda = 100$ and interpolated onto a common wavelength scale. Observational data are normalized in 0.9–1.0 μm range while models are normalized so as to minimize residuals. Best-fit parameters are listed in Table 3. (Right) Comparison of best-fit models (based on full spectrum) to observed data in the red optical. Here, both models and spectra have been smoothed to a resolution $\lambda/\Delta\lambda = 1000$ and interpolated onto a common wavelength scale. The goodness-of-fit statistic Γ computed over the 6400–9000 \AA range is notably worse than that for the full optical/near-infrared spectrum.

TABLE 1
PROPERTIES OF
SDSS J125637.13-022452.4.

Parameter	Value	Ref.
α_{J2000}	$12^h 56^m 37^s.16$	1
δ_{J2000}	$-02^\circ 24' 52''.2$	1
Spectral Type	sdL3.5	2
$i' - J$	3.253 ± 0.024	3,4
$J - K_s$	0.097 ± 0.026	4
M_J^a	12.23 ± 0.22	2,5
M_H^a	11.81 ± 0.23	2,5
$M_{K_s}^a$	11.75 ± 0.25	2,5
d_{est} (pc) ^b	66 ± 9	2,4,5
V_{tan} (km s ⁻¹)	186 ± 26	2,4
V_r (km s ⁻¹)	-130 ± 11	2
U (km s ⁻¹)	-115 ± 11	2
V (km s ⁻¹)	-101 ± 18	2
W (km s ⁻¹)	-150 ± 9	2
T_{eff} (K)	$\sim 2100-2500$	2
$\log g$ (cgs)	$\sim 5.0-5.5$	2
[M/H] (dex)	$\sim -1.5 - -1.0$	2

REFERENCES. — (1) 2MASS (Skrutskie et al. 2006); (2) This paper; (3) SDSS (Adelman-McCarthy et al. 2008); (4) Schilbach, Röser & Scholz (2009); (5) Cushing et al. (2009).

^a Estimated absolute magnitudes based on the absolute magnitude/spectral type relations of Cushing et al. (2009) and spectral type sdL3.5.

^a Note that Schilbach, Röser & Scholz (2009) measure an astrometric distance of 90 ± 23 pc for this source, formally consistent with our more precise estimate based on the Cushing et al. (2009) absolute magnitude/spectral type relations.

TABLE 2
ATOMIC LINE EQUIVALENT WIDTHS
(EW).

Feature	Line Center (Å)	EW (Å)
H α	...	>-0.9
Ca I	6571.10	3.1 ± 0.6
Ti I	7204.47	2.4 ± 0.5
Rb I	7798.41	2.9 ± 0.4
Rb I	7945.83	2.6 ± 0.2
Na I	8182.03	9.1 ± 0.2^a
Na I	8193.33	...
Ti I	8433.31	3.7 ± 0.3
Cs I	8519.19	1.3 ± 0.2
Ca II	8540.39	0.5 ± 0.3
Cs I	8941.47	1.1 ± 0.4

^a EW for combined doublet.

TABLE 3
SPECTRAL MODEL FITS.

Model	$\log g$ (cgs)	T_{eff} (K)	[M/H] (dex)	Γ
GAIA COND-PHOENIX	5.5	2300	-1.0	0.51
	5.5	2400	-1.0	0.53
	5.0	2400	-1.5	0.56
	5.0	2300	-1.5	0.57
	5.5	2500	-1.0	0.72
DRIFT-PHOENIX	5.0	2300	-1.5	0.64
	5.0	2200	-1.5	0.66
	5.5	2300	-1.5	0.67
	5.5	2400	-1.5	0.75
	5.5	2100	-1.5	0.76

NOTE. — Top five best fit models for combined optical and near-infrared spectrum of SDSS J1256–0224, ranked by Γ . Best-fit models are shown in Figure 6.

